THE ASTROPHYSICAL JOURNAL, 418:743–748, 1993 December 1

THE DISCOVERY OF A SUPERNOVA REMNANT EMBEDDED IN A GIANT H II REGION

SHAWN M. GORDON[2]
Harvard-Smithsonian Center for Astrophysics, and Institute for Astrophysics, University of New Mexico
ROBERT P. KIRSHNER[3]
Harvard-Smithsonian Center for Astrophysics, 60 Garden Street, MS 19, Cambridge, MA 02138
NEBOJSA DURIC
Institute for Astrophysics, University of New Mexico, 800 Yale Boulevard, N.E., Albuquerque, NM 87131
AND
KNOX S. LONG[3]
Space Telescope Science Institute, 3700 San Martin Drive, Baltimore, MD 21218
Received 1993 May 17; accepted 1993 June 9

ABSTRACT

We have combined radio, optical, and X-ray data to discover a new supernova remnant (SNR) in M33. This remnant is embedded in the giant H II region NGC 592. Our VLA-WSRT radio survey of M33 showed that NGC 592 has a nonthermal component to its radio emission. Optical images of the H II region at the KPNO 4 m allowed us to subtract the thermal source to reveal the nonthermal source. NGC 592 had also been identified in *Einstein* data as a soft X-ray source. Our *ROSAT* observation, combined with the radio and optical data, provides evidence that the X-ray source is a supernova remnant. A knot of [S II] emission was isolated in the H II region, and MMT spectra confirm that the knot has the spectrum of a supernova remnant. We use these observations to investigate the properties of the remnant and its environment. We find that this SNR is a typical middle-aged remnant except that it is expanding into dense gas of the H II region NGC 592. We also find that there is a pressure difference between the hot postshock region and the cool recombination zone. This difference may be a sign that nonthermal particles and magnetic fields provide significant pressure support in the recombination zone.

Subject headings: galaxies: individual (M33) — H II regions — radio continuum: interstellar — supernova remnants — X-rays: interstellar

1. INTRODUCTION

Understanding the evolution of supernova remnants (SNRs) and their interaction with the interstellar medium (ISM) requires complete samples of SNRs with known distances. Statistically complete samples help to determine the expansion law for remnants, the supernova (SN) rate, the generation of relativistic particles, and the effect of SNRs on the structure of the ISM. Remnants in our own Galaxy are complicated to use as statistical tools. Although the sample is large (≈ 170, Green 1991), it is primarily a radio sample. Optical studies of galactic remnants are so severely hampered by interstellar absorption that less than one-third of the radio sample has been detected optically (Smith et al. 1993). The distances to galactic remnants are also highly uncertain (Green 1991), further reducing their usefulness. In extragalactic samples, these problems can be reduced. Effects of varying interstellar absorption can be reduced by studying face-on systems, and while absolute distances may remain uncertain, all the SNRs in an extragalactic system are at essentially the same distance. Until recently, surveys of galaxies beyond the LMC and SMC at radio and X-ray wavelengths have had limited success due to sensitivity and resolution limitations, so most SNRs in these galaxies have been identified through optical imaging and spectroscopic techniques (Mathewson & Clarke 1973; D'Odorico, Dopita, & Benvenuti 1980; Blair, Kirshner, & Chevalier 1981; Mathewson et al. 1983, 1985; Dopita et al. 1984; Blair & Kirshner 1985; Long et al. 1990; Smith et al. 1993). Of the galaxies in the Local Group, the best galaxy for studies of SNRs is M33. It is nearby (840 kpc, Freedman, Wilson, & Madore 1991), nearly face-on ($i = 55°$, Garcia-Gomez & Athanassoula 1991), and is a spiral galaxy allowing comparisons with the Milky Way. To this end, we have undertaken new radio, X-ray, and optical observations of M33 to establish well-defined and nearly complete samples of SNRs at several wavelengths. The radio and X-ray observations are significantly more sensitive with better resolution than previous surveys (D'Odorico, Goss, & Dopita 1982; Goss & Viallefond 1985; Viallefond et al. 1986; Reynolds and Fix 1987; Long, Helfand, & Grabelsky 1981; Trinchieri, Fabbiano, & Peres 1988) and have resulted in the detection of many new sources, some of which are undoubtedly SNRs.

Optically, SNRs are identified as shock-heated emission nebulae with [S II]:Hα ratios which exceed 0.4 (Mathewson & Clarke 1973; Raymond 1979; Long et al. 1990). H II regions, on

[1] Based partly on observations obtained at the Very Large Array, the Westerbork Synthesis Radio Telescope, the ROSAT Observatory, the Kitt Peak 4 m telescope, and the Multiple Mirror Telescope Observatory. The National Radio Astronomy Observatory is operated by Associated Universities, Inc., under cooperative agreement with the National Science Foundation. The Westerbork Synthesis Radio Telescope is operated by the Netherlands Foundation for Research in Astronomy (NFRA) with financial support from the Netherlands Organization for the Advancement of Research. The Multiple Mirror Telescope Observatory is a joint facility of the Smithsonian Astrophysical Observatory and the University of Arizona.

[2] SAO Predoctoral Fellow. Postal address: Harvard Smithsonian Center for Astrophysics, 60 Gården Street, MS 10, Cambridge, MA 02138.

[3] Guest Observer at Kitt Peak National Observatory, operated by AURA, Inc., under contract to the National Science Foundation.

the other hand, typically have [S II]:Hα ≈ 0.1. Recently, Long et al. (1990) used CCD interference filter images of the inner portion of M33 to increase the number of known remnants in M33 to over 50. Follow-up spectroscopic observations with the Multiple Mirror Telescope (MMT) confirmed that the candidates were SNRs (Smith et al. 1993). Despite the success of the interference filter survey, it is quite clear that some SNRs are missed, particularly those SNRs located in or superposed on bright H II regions.

At radio wavelengths, SNRs are distinguished from H II regions by their steep, nonthermal radio spectral index ($\alpha > 0.2$, where $S_\nu = \nu^{-\alpha}$). High-resolution, sensitive radio observations of M33 have been taken with the Very Large Array (VLA) and Westerbork Synthesis Radio Telescope (WSRT) by Duric et al. (1993). They searched for radio emission from optically identified SNRs and found that 27 out of 52 optically selected SNRs could also be detected at radio wavelengths. This result suggests that many more radio-emitting SNRs can be identified with the new observations in areas where the optical surveys are incomplete or confused. We have identified an additional ≈120 nonthermal radio sources within 20′ of the center of M33 from these data. Although a few of these sources are likely to be background radio galaxies, others are certainly SNRs.

This paper describes observations of one nonthermal source from the radio survey, a source (hereafter 013022+30233) which is part of the giant H II region of NGC 592. We used new optical interference images to separate the nonthermal from the thermal radio emission in NGC 592 and to show that a compact nonthermal radio source is coincident with a knot of optical emission that is strong in [S II]. Optical spectra of the knot demonstrate that it is shock-heated, and we conclude that this source is indeed a SNR. NGC 592 had been detected as a soft X-ray source with *Einstein* (Long et al. 1981), but the X-ray source was not identified as a SNR because of poor optical data. Here, we also describe new *ROSAT* observations of NGC 592 which give convincing evidence that the X-ray emission results from a SNR. Finally, we use the radio, optical, and X-ray observations to describe the properties and environment of this new SNR. The results show the importance of a multiwavelength approach to finding extragalactic SNRs and determining their characteristics.

2. OBSERVATIONS

2.1. *Radio*

Observations of M33 were carried out at 6 cm and 20 cm (4.84 GHz and 1.42 GHz) with the VLA and the WSRT (Duric et al. 1993). The fields are approximately 40′ in diameter with a resolution of 7″ and a noise level, σ, of 35–50 μJy beam^{-1}. Following Duric et al. (1993), we have used a method analogous to aperture photometry to identify all sources with fluxes $\geq 3\ \sigma$. Because missing short spacing flux could result in a negative bowl under a source and superposed emission from a spiral arm could act as a positive background, the local background was fitted with a tilted plane and removed from the source. We were surprised to find that the total flux from the H II region NGC 592 had a nonthermal spectral index, $\alpha = 0.25 \pm 0.10$ (see Table 1).

Despite the nonthermal spectral index of the radio source, there must be a thermal bremsstrahlung contribution to the emission because of its location in an H II region. To isolate the nonthermal emission, we follow the method described by Duric et al. (1993) to separate nonthermal from thermal emission using an Hα image. We assume uniform local extinction and that line emission of the H II region dominates that of the SNR in the Hα image. The ratio of free-free to Balmer line emission is independent of density and only weakly dependent on temperature (Osterbrock & Stockhausen 1960), so the Hα image (described in more detail below) can be used to estimate the thermal component of the radio emission. The Hα image was smoothed to the resolution of the radio images and scaled to the 6 cm image such that when the scaled Hα image was subtracted from the radio image no negative residuals remained. The scaled Hα image was extrapolated to 20 cm assuming a thermal radio spectral index ($\alpha = 0.1$) and removed from the 20 cm image.

TABLE 1

RADIO PROPERTIES OF NGC 592

Component	S_{20} (mJy)	S_6 (mJy)	α
Total	4.9 ± 0.6	3.6 ± 0.4	0.25 ± 0.1
013022+30233	1.1 ± 0.6	0.41 ± 0.4	0.8 ± 0.1
Thermal	3.8 ± 0.6	3.2 ± 0.4	0.1

The results of this are shown in Figure 1 (Plate 13) and the radio flux of the thermal and nonthermal components are summarized in Table 1. The errors quoted are the rms errors of the maps and do not include systematic uncertainties resulting from our subtraction method. A compact nonthermal source remains in both 20 cm and 6 cm images (Figs. 1*c* and 1*d*) and is located at R.A. = $1^h30^m22^s.4$, Decl. = +30°23′19″. The source is marginally resolved with a diameter of 5″, estimated by deconvolving the clean beam from the residual 6 cm and 20 cm images. This corresponds to a diameter of 20 pc at the distance of M33. The peak of the nonthermal radio source is 2″ from the centroid of the X-ray source as measured with the *Einstein* HRI (Markert & Rallis 1983), coincident to within the 4″ error circle of the HRI detector.

In summary, the radio emission from NGC 592 has two components: a diffuse thermal emission from the H II region, and a compact nonthermal object whose radio spectrum is typical of SNRs and is coincident with the X-ray source.

2.2. *Optical*

We have new interference filter images obtained with the 2048 × 2048 Tektronix CCD on the Kitt Peak 4 m, observed in three bands centered on 6100 Å, Hα, and [S II] λλ6717, 6731 with FWHM equal to 143, 34, and 50 Å, respectively. A 60″ × 60″ tile centered on the nonthermal radio source was extracted from each image. Each tile was boxcar-smoothed with a 1.″5 box to suppress cosmic-ray events, decrease the noise, and lessen the effect of changes in seeing among the images. Following the method described by Long et al. (1990), the continuum image (6100 Å) was scaled and removed from the [S II] and Hα images along with a uniform background. A ratio map was formed by dividing the [S II] image clipped at the 3 σ level by the similarly clipped Hα image. These images are presented in Figure 2 (Plate 14). NGC 592 appears to be a typical H II region. However, careful scrutiny of the ratio image (Fig. 2*d*) reveals a knot of bright [S II] emission coincident with the nonthermal radio source. The coincidence of this knot with the nonthermal radio source is emphasized in Figure 3.

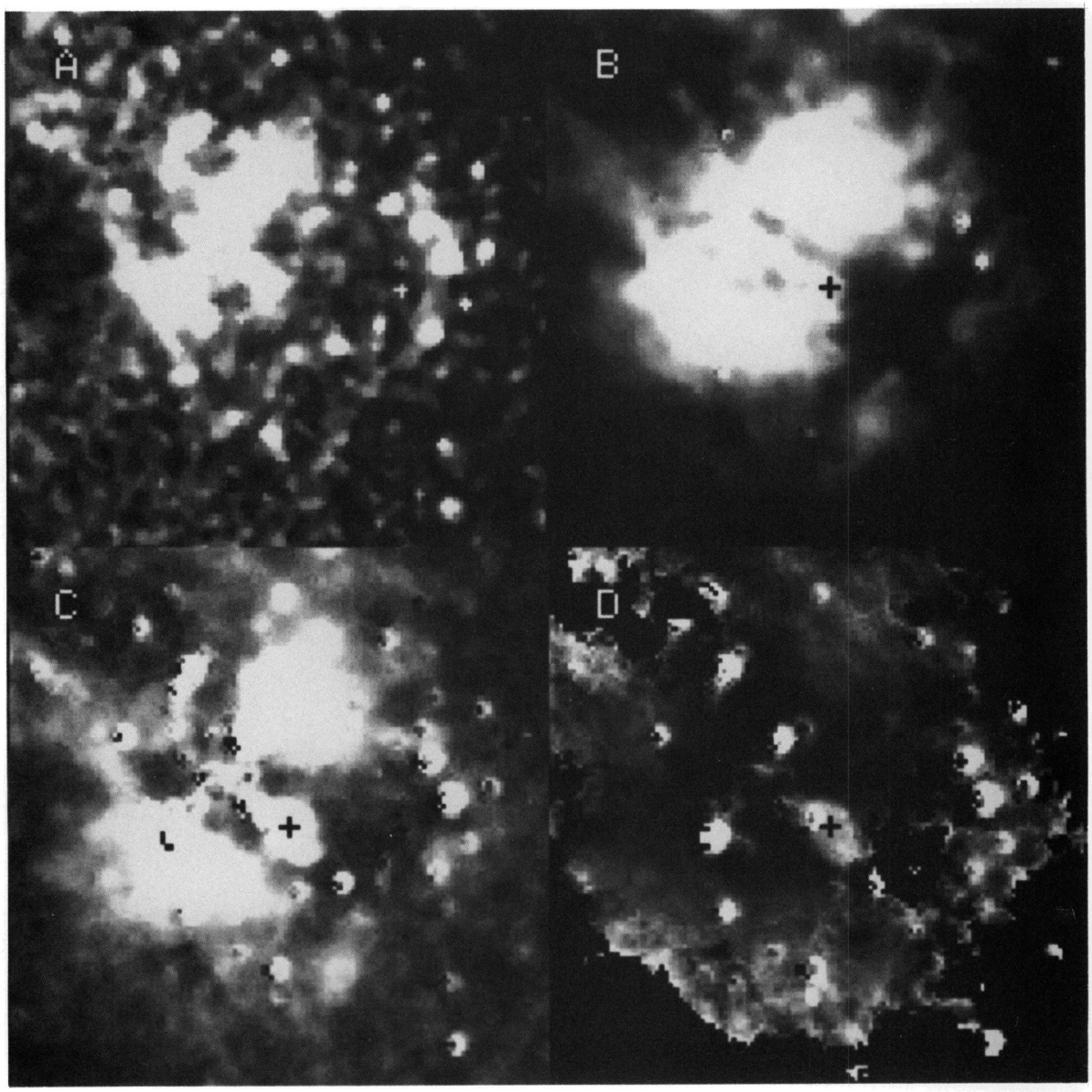

FIG. 1.—(*a*) 20 cm and (*b*) 6 cm radio images of NGC 592. Residual (*c*) 20 cm and (*d*) 6 cm radio images after the thermal contribution has been removed.

GORDON et al. (see 418, 744)

PLATE 14

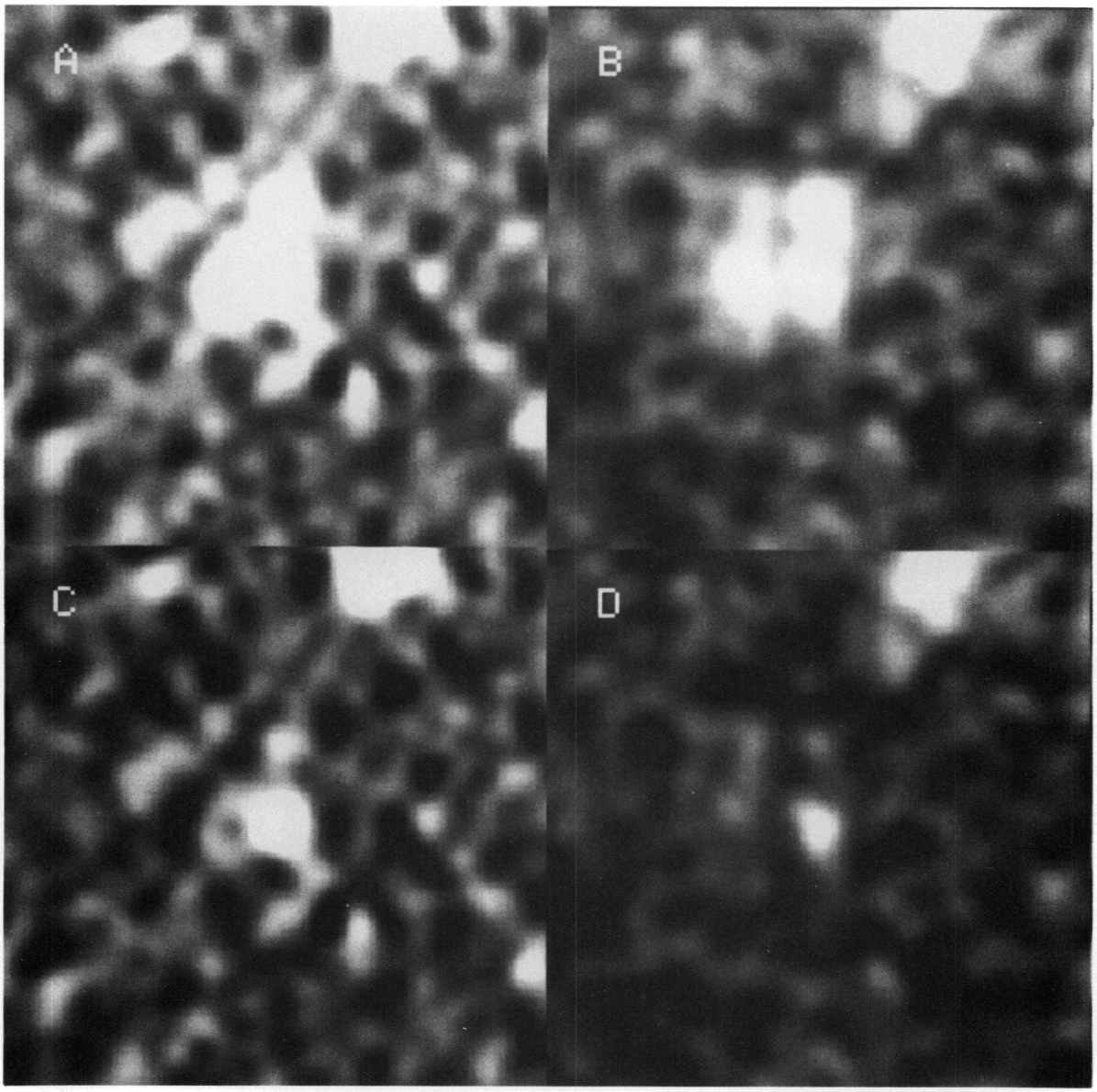

FIG. 2.—(*a*) 6100 Å image, (*b*) the continuum-subtracted Hα image, (*c*) the continuum-subtracted [S II] image, and (*d*) the [S II]/Hα map clipped at the noise levels in the Hα and [S II] images. Crosses emphasize the location of the SNR.

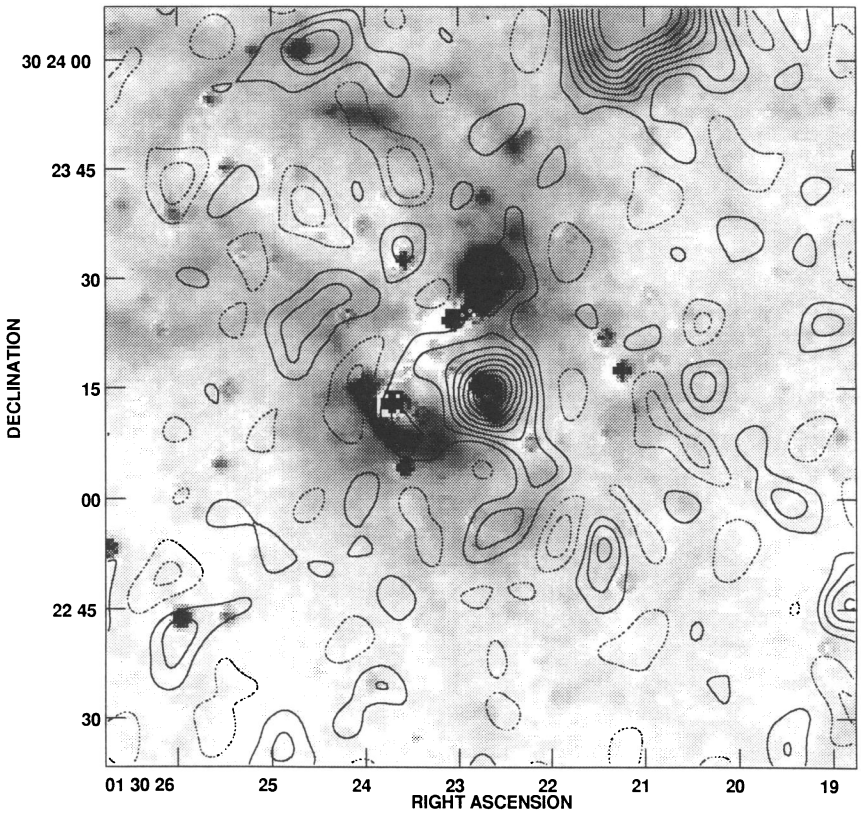

FIG. 3.—This is an overlay of a contour map of the nonthermal component of the 20 cm radio emission on a grayscale of the continuum-subtracted [S II] emission. Notice that the peak knot of radio emission is coincident with the bright [S II] knot. Contour levels are multiples of 3 times the local rms.

Averaging over a 2".5 × 2".5 box, we estimate the value of [S II]/Hα to be ≈0.5 in the images.

We obtained a spectrum of the knot with the MMT on 1991 October 15 using the Red Channel long-slit CCD spectrograph (Schmidt, Weymann, & Foltz 1989). The set-up, described by Smith et al. (1993), provided a resolution of approximately 7 Å with spectral coverage from 6200 Å to 7500 Å and allowed the separation of the [N II] lines from Hα and resolved the density sensitive [S II] lines. The 2" × 180" slit allowed us to obtain a spectrum of the candidate, the background emission in which the candidate is embedded, and adjacent filaments of the H II region for comparison. Two observations of 30 minutes each were taken of the SNR candidate with the slit aligned east to west.

Spectra for the knot and H II region are presented in Figures 4*a* and 4*b*. Line strengths for all detectable lines were determined as described by Smith et al. (1993) and are included in Table 2. For comparison, we also include the typical SNR line strengths for a filament in the LMC remnant N49 (Vancura et al. 1992). With [S II]/Hα = 0.59, the optical emission of the knot is typical of the shock-heated gas seen in SNRs. In contrast, the H II region has [S II]/Hα = 0.07, typical of a photoionized region. The forbidden lines of [O I] λ6300 and λ6363, which are usually much stronger in shock-heated gas than in photoionized gas, were also detected in the knot spectrum, whereas no emission from these lines is detectable in the H II region. Since it is unlikely that all of the Hα emission due to the surrounding H II region was removed, the line ratios of the SNR represent lower limits to the true values. We conclude that the optical emission of 013022+30233 has the spectrum of a SNR.

The density-sensitive [S II] lines were used to estimate the density in the recombination zone. This should represent the typical density of the cool clouds that the shock front has encountered. Using the relation between the [S II] electron density and λ6717/λ6731 (Blair & Kirshner 1985), we find a rather high value of N[S II] ≈ 270 cm^{-3} (see Table 3). Assuming that the recombination zone is at 10^4 K, the pressure is 2.7 × 10^6 cm^{-3} K.

TABLE 2

LINE STRENGTHS

Line	013022+30233	NGC 592	N49[a]
[O I] λ6300	18.9	<1.0	89.6
[O I] λ6363	7.4	<1.0	30.0
[N II] λ6548	19.2	4.7	19.8
Hα λ6563	300.0[b]	300.0[c]	300.0
[N II] λ6584	57.6	14.1	69.3
[He I] λ6678	6.1	3.3	2.8
[S II] λ6717	75.9	9.8	89.8
[S II] λ6731	69.9	8.4	121.0
[Ar III] λ7135	7.5	3.5	4.0
[Fe II] λ7155	6.3	<1.0	12.6
[Ca II] λ7291	3.9	<1.0	20.4
[O II] + [Ca II] λ7325	17.7	<1.0	41.8

[a] Vancura et al. 1992.
[b] F(Hα) = 1.5 × 10^{-14} ergs s^{-1} cm^{-2}, through a 2" × 5" aperture.
[c] F(Hα) = 2.5 × 10^{-14} ergs s^{-1} cm^{-2}, through a 2" × 4" aperture.

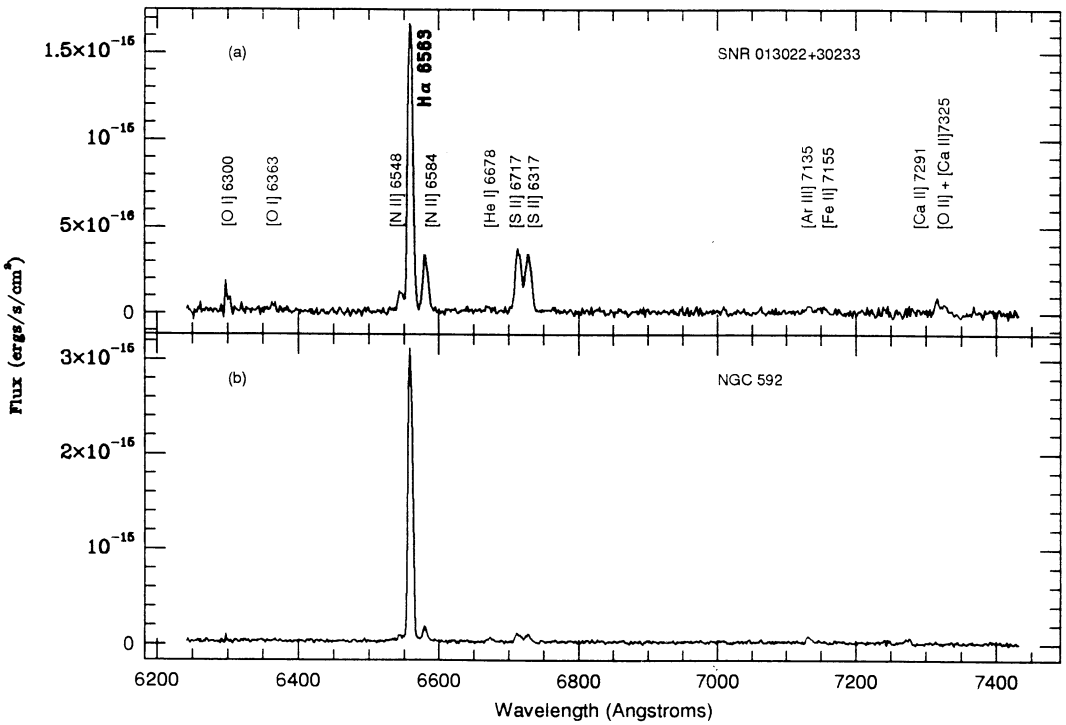

FIG. 4.—(*a*) Spectrum of the knot of optical emission coincident with the nonthermal radio source. Note the high ratio of [S II] to Hα as compared to (*b*), and the detection of [O I]. (*b*) Spectrum of the H II region away from the nonthermal radio source.

2.3. *X-Ray*

M33 was observed with the PSPC detector on *ROSAT* for 30 ks on 1991 August 20 (Long 1993). We detected the strong source coincident with NGC 592. Its X-ray spectrum is soft, $R = -0.5$, where R, the hardness ratio, is the ratio of the difference to the sum of the count rates in the 1.0–2.5 keV band and the 0.08–1.0 keV band. At 4.1×10^{37} ergs s^{-1}, it is one of the most luminous sources in M33 and is the most luminous soft X-ray source in the central 40′ of M33. Since most of the soft X-ray sources are SNRs, the source in NGC 592 is probably the brightest SNR in M33.

To determine the density and temperature of the postshock gas, we modeled the spectrum of this source using the PROS software package in IRAF. Because of uncertainties in the vignetting correction in the lowest energy bins and lack of counts in the highest bins, the spectrum was fitted using channels 10 through 25, corresponding to an energy range of 0.37 keV–1.5 keV. Both a power law and a Raymond thermal spectrum (Raymond & Smith 1997) were fitted to the data, but the power-law spectrum did not yield satisfactory results. The Raymond thermal spectrum allows three parameters to be fitted with fixed abundances: the foreground column density, $n_{\rm H}$, the temperature of the postshock region, $T_{\rm ps}$, and the volume emission measure, EM. The metal abundances were fixed to 0.25 solar, appropriate for M33 (Kwitter & Aller 1981), and a Morrison-McCammon model (1983) was used for the absorption. The intrinsic column density has been estimated from the H I map of M33 (Deul & van der Hulst 1987) to be 10^{21} cm^{-2} in the direction of NGC 592 and the galactic column density, interpolated from Stark et al. (1992) with the Einline package COLDEN, in the direction of M33 is estimated to be 6×10^{20} cm^{-2}. Since this source, in all likelihood, resides in M33, we constrain the column density to be the sum of the galactic and half the intrinsic column densities, $\log (n_{\rm H}) = 21.04$, and fit only the normalization and the temperature. The minimum χ^2 ($=18.5$) was reached for $T_{\rm ps} = (3.8 \pm 0.9) \times 10^6$ K and $\log (EM/{\rm cm}^{-3}) = 60.63 \pm 1.1$, where the errors have been determined from the 95% χ^2 confidence intervals. The flux and luminosity are then estimated to be 4.8×10^{-13} ergs cm^{-2} s^{-1} and 4.1×10^{37} ergs s^{-1}, respectively. With a reduced $\chi^2 \approx 1$, the model is a good fit to the observation. This result would be expected from a hot ($\approx 10^6$ K) thin plasma such as the postshock region in an SNR.

The volume emission measure can be used to estimate the density of the X-ray emitting postshock region. The postshock density, $n_{\rm ps}$, is related to the volume emission measure via $EM = n_{\rm ps}^2 V$, where V is the volume of the X-ray emitting region. Because all confirmed Crab-like remnants have flat radio spectral indices (Green 1988), the nonthermal radio spectral index indicates that 013022+30233 is a shell-like remnant. Therefore, if we assume that the compression behind the shock is a factor of 4, the thickness of the shell is $\approx 1/12$ the radius. Then, using the optical diameter of 28 pc as the approximate size of the remnant, the postshock density is $n_{\rm ps} = 7.1$ cm^{-3}, and assuming the postshock gas is ideal, the postshock pressure is $P_{\rm ps} = 2.9 \times 10^7$ cm^{-3} K.

The X-ray source in NGC 592 is a soft X-ray source whose spectrum can be modeled by a thermal bremsstrahlung spectrum with line emission and is consistent with its emission being from an SNR. The results of this analysis are summarized in Table 3.

3. DISCUSSION

Information derived from the radio, optical, and X-ray observations can be used to determine the characteristics of the remnant and its environment. A summary of the observed and

TABLE 3

SNR PROPERTIES

Wavelength	Property	013022 +30233	Cygnus Loop	N49	Units
Optical	D	28	40[a]	17[b]	pc
	n(S II)	270	120[c]	150[d]	cm^{-3}
Radio	D	20	40[a,e]	16[e]	pc
	L_R	13.3	4.2[f]	137.7[b]	10^{33} ergs s^{-1} (0.01–100 GHz)
	E_{nt}	8.3	4.2	9.3	10^{49} ergs
X-ray	EM	4.2	0.2[g]	0.3[g]	10^{60} cm^{-3}
	T_{ps}	3.8	3.00[h]	7.5	10^6 K
	L_x	4.1	0.1[h]	2.4[d]	10^{37} ergs s^{-1} (0.08–2.4 keV)
	P_{ps}	2.9	0.19	5.4	10^7 cm^{-3} K
	n_0	1.8	0.16[h]	0.9[d]	cm^{-3}
	V_s	520	400[h]	730[d]	km s^{-1}
	E_0	2.1	0.3[h]	1.0[d,i]	10^{51} ergs
	τ	11.0	18.0[h]	5.4[d]	10^3 yr

[a] Assuming distance = 770 pc.
[b] Mathewson et al. 1983.
[c] Fesen, Blair, & Kirshner 1982.
[d] Vancura et al. 1992.
[e] Mills et al. 1984.
[f] Green 1988.
[g] Assuming $EM = (4n_0)^2V$.
[h] Ku et al. 1984.
[i] Assumed parameter.

derived properties for this remnant is presented in Table 3. Included are the properties of the Cygnus Loop and the LMC remnant N49, two classic examples of remnants expanding into distinctly different media. The Cygnus Loop is generally believed to be encountering cool dense clouds with typical densities of 5–10 cm^{-3} in an ISM with a density of $\approx$0.1 cm^{-3} (DeNoyer 1975). N49, on the other hand, appears to be associated with a faint H II region and is interacting with a large molecular cloud (Chu & Kennicutt 1988). In § 3.1, we use the X-ray observations to show that 013022+30233 is more like the SNR N49 than the Cygnus Loop, and in § 3.2, we use the optical, X-ray and radio observations to understand the role of relativistic particles and magnetic fields in supporting the gas in the postshock medium.

3.1. *X-Ray Properties*

Assuming that the shock is strong, the preshock density, n_0, is one-fourth the postshock density. Comparing n_0 in 013022+30233 to the Cygnus Loop and N49, we see that 013022+30233 is expanding into a denser ISM than the Cygnus Loop, and one that is similar to the medium around N49. Thus, 013022+30233, like N49, is encountering a high density surround: in this case the H II region NGC 592.

The postshock temperature and density, along with the optical diameter, D, can be used to estimate the initial blast energy, E_0, current shock velocity, V_s, and age, τ, of the remnant. The optical diameter indicates that this remnant is a middle-aged remnant, so we assume that it is in the adiabatic stage of evolution. We continue to assume it is a shell-like remnant with a thickness that is 1/12 of its radius. For a strong shock, T_{ps} yields the shock velocity (see McKee & Hollenbach 1980), and the Sedov (1959) equations can be used to estimate the age and initial blast energy of the remnant. The shock velocity of $\approx$540 km/s and age of $\approx$9800 yr indicate that this remnant is typical of other middle-aged remnants such as the Cygnus Loop and N49. The inferred blast energy of 013022+30233 is higher than that estimated for the Cygnus Loop and is approximately equal to the assumed blast energy of N49.

The location of 013022+30233 in an H II region has had a significant effect on its properties. Since the emissivity is proportional to the square of the density, its location in a dense medium result in a high emissivity and is the major reason why this SNR is so luminous at X-ray wavelengths. In addition, the surrounding H II region has resulted in more mass being swept up by the shock front and has led to a significant deceleration of the remnant compared to the Cygnus Loop.

3.2. *Nonthermal Pressure Support in the Remnant*

When only an optical spectrum is available, the typical method for determining the postshock pressure is to assume that the pressure in the cool gas of the recombination zone is in pressure equilibrium with the hot postshock gas. However, as has been pointed out by Raymond et al. (1988) and Vancura et al. (1992), there appears to be a difference between the pressure in the recombination zone and the postshock pressure in both the "spur" of the Cygnus Loop and in N49. The X-ray spectrum measures the density and temperature of the hot postshock gas, while the [S II] lines measure the pressure in the cool gas. Using our observations, we find a similar difference in the pressures in 013022+30233. The pressure in the hot postshock region is 10 times that of the pressure in the dense clouds. Raymond et al. (1988) hypothesized that the difference in pressures could be accounted for by a nonthermal plasma. Since the radio observations measure the energy content of relativistic particles and magnetic fields in the SNR, we can use our radio observations of 013022+30233 to estimate the pressure support due to the nonthermal plasma.

The nonthermal pressure, P_{nt}, due to relativistic particles and magnetic fields in a radio-emitting plasma can be written as

$$P_{nt} = \frac{1}{3}\frac{E_{nt}}{V}, \quad (1)$$

where E_{nt} is the total energy of the relativistic particles and magnetic fields, and V is the volume of the emitting region. For our case, we assume, as before, that the radio emission is confined to a shell whose thickness is 1/12 of the radius, yielding a volume-filling factor of 25%. If the relativistic particles and magnetic fields are in equipartition then the nonthermal energy is approximately equal to the minimum energy of the field and particles. The nonthermal energy is given by (see Pacholczyk 1970):

$$E_{nt} = 1.05 \times 10^4(1 + k)^{4/7}V^{3/7}L_r^{4/7}, \quad (2)$$

where L_r is the radio luminosity between 0.01 GHz and 100 GHz, and $k \approx 100$ is the ratio of relativistic protons to electrons.

We find that the nonthermal energy is 8.3×10^{49} ergs, corresponding to a nonthermal pressure of $P_{nt} = 2.4 \times 10^6$ cm^{-3} K. This pressure is significantly less than the pressure in the postshock gas, as estimated from the X-ray observation, and apparently cannot account for the difference between the postshock pressure and the pressure in the recombination zone. However, the pressure determined in this manner represents the minimum pressure of relativistic and magnetic fields, and any departure from equilibrium between particles and mag-

netic fields will increase the nonthermal pressure. In addition, the filling factor of radio emission, a major source of uncertainty in this argument, is unlikely to exceed 25% of the volume of the SNR, and in fact may be a smaller fraction of the volume. Any decrease in the volume-filling factor will also increase the nonthermal pressure. So, the nonthermal pressure could play a dominant role in the recombination regions of an SNR if equipartition does not hold between relativistic particles and magnetic fields or if our estimate of the filling factor is too high. In any case, the nonthermal pressure is comparable to the pressure as determined from the [S II] lines for an assumed temperature of 10^4 K in the recombination zone, and thus plays a significant, if not dominant, role in the support of the gas in the dense clouds.

4. CONCLUSION

We have shown that the giant H II region, NGC 592, in M33 contains a SNR. Evidence for the embedded SNR was found at optical, radio, and X-ray wavelengths. A nonthermal radio source was isolated in the NGC 592 and was found to be coincident with a knot of bright [S II] emission and a X-ray source detected by the *Einstein* and *ROSAT* observatories. An optical spectrum of the knot showed that the emission is characteristic of shock-heated gas. Finally, the X-ray emission is soft and well fitted by a Raymond thermal spectrum with a temperature of 4×10^6 K, typical of the X-ray emission seen from a SNR.

Our results demonstrate the power of applying sensitive observations at multiple wavelengths to identify and to study the properties of remnants in external galaxies. Confusion by Hα emission prevented this SNR from being caught in optical surveys of M33, and the H II region obscured the potential identification from the *Einstein* data. Radio observations show that NGC 592 contains a nonthermal radio source. We used the Hα emission of NGC 592 to remove the thermal emission from the 20 cm and 6 cm images. The result is the compact nonthermal radio source coincident with the soft X-ray emission and the bright [S II] knot. We will use this approach as the prototype for future searches of embedded SNRs.

The X-ray spectrum indicates that 013022+30233, which resembles the LMC remnant N49, is a typical middle-aged remnant expanding the H II region NGC 592. The difference observed between the pressure in the postshock medium and the pressure of the recombination zone may be resolved, at least in part, by nonthermal pressure of relativistic particles and magnetic fields.

We thank J. Raymond for many useful discussions. We also thank J. Hughes and F. Seward for their help in the reductions and analysis of the *ROSAT* data. This work has been supported by NSF grant AST 89-05529 and by *ROSAT* grant NAG5-1539.

REFERENCES

Blair, W. P., & Kirshner, R. P. 1985, ApJ, 289, 582
Blair, W. P., Kirshner, R. P., & Chevalier, R. A. 1981, ApJ, 247, 879
Chu, Y.-H., & Kennicutt, R. C. 1988, ApJ, 96, 1874
DeNoyer, L. K. 1975, ApJ, 196, 479
Deul, E. R., & van der Hulst, J. 1987, A&AS, 67, 509
D'Odorico, S., Dopita, M. A., & Benvenuti, P. 1980, A&AS, 221, 67
D'Odorico, S., Goss, W., & Dopita, M. A. 1982, MNRAS, 198, 1059
Dopita, M. A., Binette, L., D'Odorico, S., & Benvenuti, P. 1984, ApJ, 276, 653
Duric, N., Viallefond, F., Goss, W. M., & van der Hulst, J. M. 1993, A&AS, 99, 217
Fesen, R. A., Blair, W. P., & Kirshner, R. P. 1982, ApJ, 262, 171
Freedman, W. L., Wilson, C., & Madore, B. 1991, ApJ, 372, 455
Garcia-Gomez, C., & Athanassoula, E. 1991, A&AS, 89, 159
Goss, W. M., & Viallefond F. 1985, J. Astrophys. Astron., 6, 145
Green, D. A. 1988, Ap. Space Sci., 148, 3
———. 1991, PASP, 103, 201
Ku, W. H.-M., Kahn, S. M., Pisarski, R., & Long, K. S. 1984, ApJ, 278, 615
Kwitter, K. B., & Aller, L. H. 1981, MNRAS, 195, 939
Long, K. S. 1993, in preparation
Long, K. S., Blair, W. P., Kirshner, R. P., & Winkler, P. F. 1990, ApJS, 72, 61
Long, K. S., D'Odorico, S., Charles, P. A., & Dopita, M. A. 1981, ApJ, 246, L61
Long, K. S., Helfand, D. J., & Grabelsky, D. A. 1981, ApJ, 248, 925
Markert, T. H., & Rallis, A. D. 1983, ApJ, 275, 571
Mathewson, D. S., & Clarke, J. N. 1973, ApJ, 180, 725
Mathewson, D. S., et al. 1983, ApJS, 51, 345
Mathewson, D. S., et al. 1985, ApJS, 58, 197
McKee, C. F., & Hollenbach, D. J. 1980, ARA&A, 18, 219,
Mills, B., Turtle, A., Little, A., & Durdin, J. 1984, Australian J. Phys., 37, 321
Morrison, R., & McCammon, D. 1983, ApJ, 270, 119
Osterbrock, D. E., & Stockhausen, R. E. 1960, ApJ, 131, 310
Pacholczyk, A. G. 1970, Radio Astrophysics, Non-Thermal Processes in Galactic and Extragalactic Sources (San Francisco: Freeman)
Raymond, J. C. 1979, ApJS, 39, 1
Raymond, J. C., Hester, J., Cox, D., Blair, W., Fesen, R., & Gull, T. 1988, ApJ, 324, 869
Raymond, J. C., & Smith, B. W. 1977, ApJS, 35, 419
Reynolds, S. P., & Fix, J. D. 1987, ApJ, 322, 673
Sedov, L. 1959, Similarity and Dimensional Methods in Mechanics (New York: Academic)
Schmidt, G. D., Weymann, R. J., & Foltz, C. B. 1989, PASP, 101, 713
Smith, R. C., Kirshner, R. P., Blair, W. P., Long, K. S., & Winkler, P. F. 1993, ApJ, 407, 564
Stark, A. A., et al. 1992, ApJS, 79, 77
Trinchieri, G., Fabbiano, G., & Peres, G. 1988, ApJ, 325, 531
Vancura, O., Blair, W., Long, K., & Raymond, J. 1992, ApJ, 394, 158
Viallefond, F., Goss, W., van der Hulst, J., & Crane, P. 1986, A&AS, 64, 237